HAL
open science

Selectively boron doped homoepitaxial diamond growth for power device applications

F. Lloret, D. Eon, Etienne Bustarret, F. Donatini, D. Araujo

To cite this version:

F. Lloret, D. Eon, Etienne Bustarret, F. Donatini, D. Araujo. Selectively boron doped homoepitaxial diamond growth for power device applications. Applied Physics Letters, 2021, 118 (2), pp.023504. 10.1063/5.0031478 . hal-03361210

HAL Id: hal-03361210

https://hal.science/hal-03361210v1

Submitted on 1 Oct 2021

HAL is a multi-disciplinary open access archive for the deposit and dissemination of scientific research documents, whether they are published or not. The documents may come from teaching and research institutions in France or abroad, or from public or private research centers.

L'archive ouverte pluridisciplinaire **HAL**, est destinée au dépôt et à la diffusion de documents scientifiques de niveau recherche, publiés ou non, émanant des établissements d'enseignement et de recherche français ou étrangers, des laboratoires publics ou privés.

Selectively boron doped homoepitaxial diamond growth for power device applications

F. Lloret[1], D. Eon[2], E. Bustarret[2], F. Donatini[2] and D. Araujo[3]

[1] *Department of Applied Physics, University of Cádiz, 11510, Puerto Real (Cádiz), Spain*

[2] *Univ. Grenoble-Alpes, Institut Neél, 38000, Grenoble, France*

[3] *Department of Material Science, University of Cádiz, 11510, Puerto Real (Cádiz), Spain*

fernando.lloret@uca.es

ABSTRACT

Diamond lateral growth is a powerful technique for the design and fabrication of diamond-based power electronic devices. Growth orientation affects the diamond deposition in terms of growth rate, surface roughness and impurities incorporation. It has been shown that the final grown surface of a patterned substrate can be pre-designed based on the growth conditions. Thus, simultaneous growth along different surface orientations yields regions with different properties. In line with this, the incorporation of boron in a MW PE CVD laterally deposited epilayer over a mesa patterned {100}-oriented diamond substrate was studied by cathodoluminescence. It was observed that laterally oriented facets were highly boron doped in contrast to the {100}-oriented surfaces which did not show any bound exciton emission, related to the doping. This study shows that, by designing the initial pattern and tuning the conditions, it is possible to drive a selective incorporation of boron into the grown layer.

Diamond has been widely claimed to be the ultimate semiconductor for power device applications. However, the improvement of power electronics not only depends on the intrinsic characteristics of the semiconductor, but also on the architecture of the device [1, 2]. A decisive improvement of its electrical characteristics, is expected from a three-dimensional (3D) design. 3D architectures allow to reduce the electric field within the material, which enables operation at higher voltages. Moreover, better material qualities (dopant incorporation, generation of defects, …) can be achieved by using other growth directions (such as <111>, or <311>) combined with that of the substrate [3]. 3D devices offer many advantages, such as low-specific on-resistance ([4]), a high breakdown voltage (VB) and a smaller size [4,5,6].

These features have aroused interest in developing devices based on mesa structures [5-10]. Recently, lateral diamond growth has been proposed for the purpose [11, 12]. These works showed that, by tuning the growing conditions, it was possible to grow along a specific orientation on patterned substrates. This method is not only valid for the design of new architectures but also for the control and reduction of dislocations [13, 14].

In this contribution, the effect of lateral growth on the incorporation of impurities is evaluated. A thin boron-doped layer grown laterally over a mesa patterned substrate was investigated by cathodoluminescence (CL). Boron doping modifies the electronic properties of diamond, pinning the Fermi level and incorporating acceptor levels in the bandgap, leading as the doping increases to an impurity band merging with the valence band above the metallic transition. The CL set-up collects the photon generated by the interaction of the incident electrons with the electrons in the sample. The consecutive radiative recombination spectrum depends on the electronic properties of the sample. In particular, at low temperature, excitons bound to boron impurities have specific spectral signatures that make it possible to determine the boron doping levels over a wide range [15-19]. In fact, there is a competition between free exciton and bound exciton recombination channels in the doped regions. When the CL spectrum is recorded in a doped layer, the shorter radiative lifetime of the bound excitons result in a dominant peak centered on their recombination energy, ≈5.22 eV. In diamond, due to the indirect character of the gap, the exciton recombinations involve either transverse optical (TO) or transverse

acoustic (TA) or longitudinal optical phonons. These phonons allow to match momentum and imply a weak probability of radiative recombination that results in longer radiative lifetimes. In addition, a weak bound exciton luminescence without phonon (NP) assistance is also usually observed, less intense and at a higher energy than that involving phonons [19]. In some cases, the transitions also exhibit zone center optical phonon replicas (TO+O). The latter are commonly observed in highly boron doped samples [17]. Consequently, doped regions can be easily identified by CL using the emission of the bound excitons.

For this purpose, one {100}-oriented HPHT diamond substrate from Sumitomo Electric has been etched 1 µm by inductively coupled plasma reactive ion etching (ICP-RIE) with rectangular patterns (30µm x 1mm). Pure oxygen gas was used for the plasma etching, with a 1000 W coil power, a 40 W substrate holder power, a 100 sccm gas flow, at a pressure of 10 mTorr. After chemical cleaning, the patterned substrate was homoepitaxially grown by microwave plasma enhanced chemical vapor deposition (MW PE CVD). A first undoped layer was deposited for 3 hours using a methane concentration of CH_4/H_2=0.1 % in 200 sccm total flux. A thin doped layer was then grown on top for 8 min. It was grown at CH_4/H_2=0.25% and using diborane as boron source with a concentration of [B]/[C]=2.8%. The 260 W of MW power used during the growth of both layers resulted in a temperature of 900°C as measured by an ISR 6-TI advanced infrared pyrometer from Lumasense Technologies. Working pressure was set at 33Torr for the whole process. These conditions were chosen to favor lateral growth, i.e. growth along a different orientation than the one of the substrate {100} [12]. The sample surface was studied by scanning electron microscopy (SEM) using a FESEM Zeiss Ultra plus microscope at 5 kV accelerating voltage. CL spectra were recorded at 4K using a helium cryostat in a FEI Quanta 200 SEM equipped with a parabolic mirror for collecting and focusing of the light and a Jobin Yvon HR460 grating (600 g/mm) monochromator associated to either a photomultiplier or a CCD (256×1024 matrix pixels) camera.

MW PE CVD diamond deposition under the conditions described above resulted in a lateral growth with clear faceting along the {011} orientations [20]. Figure 1 shows a SEM micrograph of the surface of the sample where part of a mesa rectangle appears after the growth process. The sample was tilted 35º to better

see the lateral growth at the edges of the mesa. In the micrographs, a lighter contrast was also evidenced. This contrast is attributed to the initial shape of the rectangle prior to any deposition. It is likely due to different local electrical characteristics related to the boron contents in the regions. Fig. 1 (a) shows one of the corners with higher detail. A second contrast, less obvious, was also observed. It is probably due to the changes in the growth orientation during the first and prolonged step of the deposition process [11, 12].

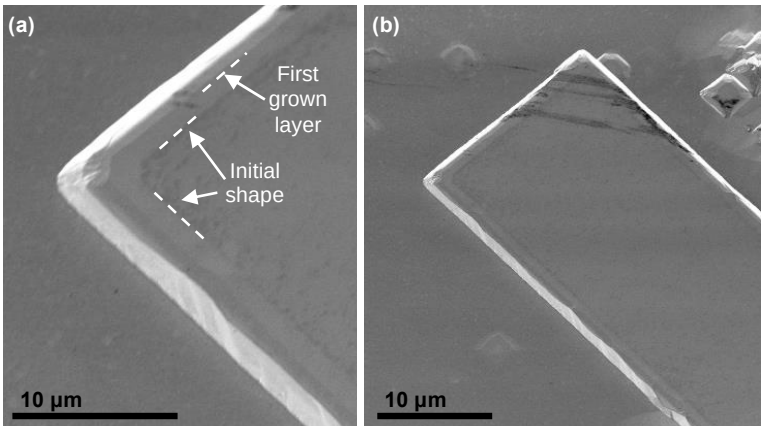

Figure 1. SEM micrographs of the grown sample tilted 35º. Two contrast are observed, one attributed to the initial shape and another, less obvious, due to the change in the surface orientation. Both are visible at the edges of the structure and marked in **(a)**.

In order to clarify this point and evaluate the boron-doped layer deposited on the top of the sample, CL spectra at different positions of the sample were recorded. Figure 2 (a) shows a SEM micrograph of the sample with the positions where the spectra were recorded marked by colored crosses and labels A, B, C and D. These positions correspond to outside (A) or within (D) the mesa rectangle, to the lateral side of the mesa (B) and to the upper corner (C). The spectra are shown in figure 2 (b), where the region of energies corresponding to the bound exciton (BE^{TO}) and free exciton (FE^{TO}) are inset enlarged. These spectra illustrate the different electrical behaviors present in the sample. A and D positions show spectra of non-doped diamond with a few weak emitter peaks, typical from bad quality substrates. In contrast, B and C shows clearly the BE^{NP}, FE^{TO} and FE^{TO+O} peaks at the energies of 5.354 eV, 5.265 eV and 5.106 eV, respectively. BE^{TO} and BE^{TO+O} peaks were detected at 5.207 eV and 5.042 eV, respectively, for B, and 5.208 eV and 5.043 eV, respectively, for C. A FE^{TO+2O} signal was also observed in both spectra at around 4.898 eV.

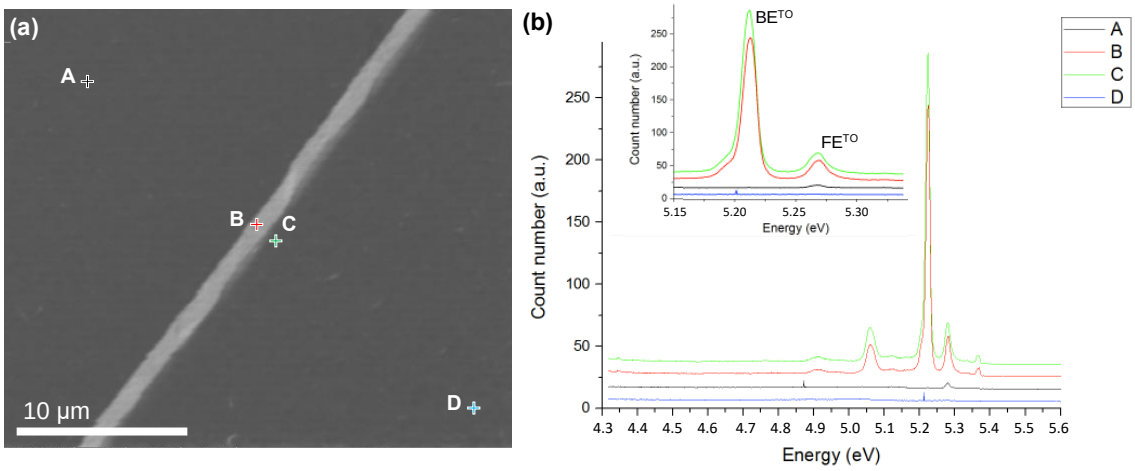

Figure 2. (a) SEM micrograph of the region where spectra are recorded with the specific positions marked. **(b)** CL spectra of the four positions shown in the SEM micrograph.

These spectra show a large bound exciton peak, characteristic of doping, only in some regions of the sample (B and C positions). However, the absence of any exciton signal in the other regions may be related to a bad crystalline quality. A high density of defects would result in a non-radiative recombination of the carriers. In order to check if the spectra obtained in A and D are due to the bad quality of the substrate in these positions, additional CL spectra have been recorded. Fig.3 shows spectra obtained at two other positions, (a) E and (b) F, marked in the SEM micrographs shown as inset. Position E, Fig.3 (a), yields a very intense FE^{TO} emission at 5.265 eV. BE^{NP}, BE^{TO} and FE^{TO+O} are also identified with lower emission at the 5.317 eV, 5.210 eV, and 5.101 eV energies, respectively. In contrast, position F, Fig.3 (b), yields a spectrum where BE^{TO} peak is the dominant exciton, with an energy of 5.208 eV. BE^{NP} (5.352 eV), FE^{TO} (5.265 eV) and BE^{TO+O} (5.046 eV) were also recorded. In both cases, excitons are observed. However, the bound exciton emission is clearly predominant in the position F, while the free exciton is the main peak at E. This shows a similar crystal quality in both regions but points to a clearly different doping level. Such doping levels can be estimated using the ratio of the BE^{TO} and FE^{TO} peaks intensities [21]. From this analysis, boron incorporated in E region (position analogous to D in Fig.2) resulted in $3x10^{15}$ cm^{-3}. This value is the minimum boron concentration expected in non-intentionally doped layers grown without boron precursors but using a reactor contaminated with residual boron atoms. Thus, for our set-up, this corresponds to usual values obtained for undoped diamond, i.e. non-intentionally doped diamond. On the other hand, carrying out the same analysis on region F resulted in a boron

content estimated at $2x10^{17}$ cm^{-3}. Both values are also in good agreement with the relationship reported by other authors between the BE^{TO} energy position and the boron incorporation [16].

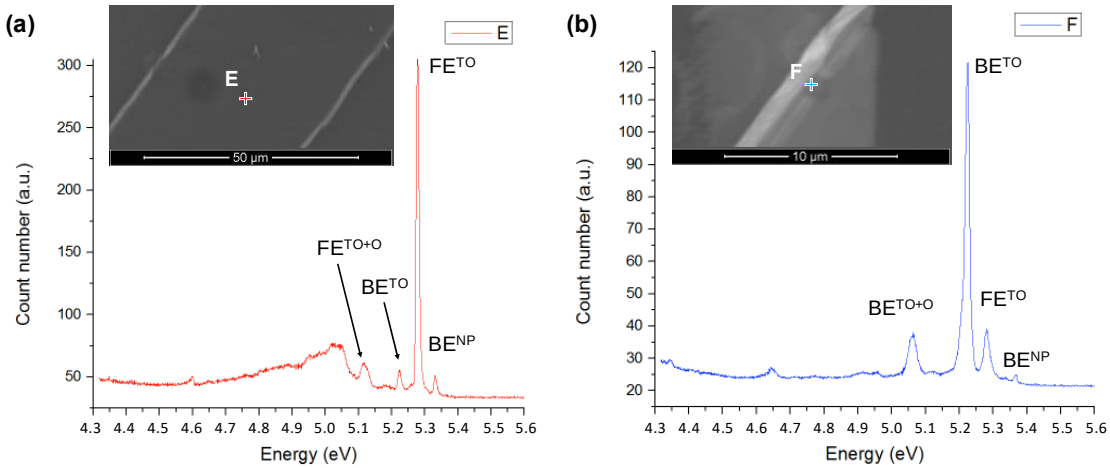

Figure 3. CL spectrum at the positions marked with a cross in the SEM micrographs shown as inset. **(a)** Spectrum recorded in an area of the sample growth vertically along the (100) orientation. **(b)** Spectrum recorded in an area of the sample growth laterally. Main peaks are identified.

To further study this growth behavior, and show this up over an extended region, monochromatic CL mapping at the BE^{TO} energy has been carried out. Fig.4 shows a region of the sample with a corner of one of the mesa rectangles by SEM in (a) secondary electron (SE) mode and (b) by monochromatic CL micrograph at 5.210 eV. The white signal in the SE image corresponds to the lateral planes of the mesa. The places where the bound exciton was detected are shown in Fig. 4 (b) with a white contrast. Monochromatic CL maps looked similar to the SEM micrographs. It is because bound exciton emissions were coming from the edges of the mesa rectangle.

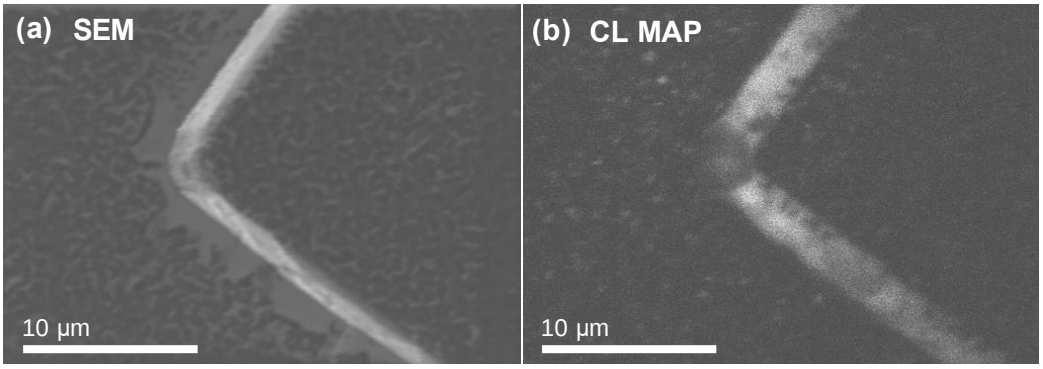

Figure 4. (a) SE-SEM micrograph of one of the corner of a mesa rectangle. **(b)** Monochromatic CL map of the BE^{TO} peak (5.210 eV) corresponding to the same region of the sample.

Therefore, the monochromatic mapping at the BE^{TO} peak energy over this sample showed a selective doping, i. e., a fully selective growth of a highly boron doped layer place exclusively present on the lateral facets. It is known that samples grown with low methane concentrations have a quite low growth rate [20]. Extrapolating growth rates for undoped diamond obtained in previous works [20], layer thicknesses of 96 nm and 8 nm are expected on the {111} lateral planes and the 100 surface orientation (i.e. at positions F and E in Fig. 3), respectively. Considering now that the layer grown was doped with boron, these thicknesses are expected to be much less [22] and, therefore, negligible on the {100} planes.

In order to determine if a 8 nm thick boron-doped diamond layer can be detected by CL, a Monte Carlo simulation has been carried out using the Casino © software. A bi-layer composed by two diamond layers, one of 8 nm thickness and another labelled substrate, has been chosen to reproduce the sample. A microscope beam acceleration voltage of 5 keV, the same value as experimentally used, was selected in order to simulate a total number of 2000 trajectories. Fig. 5 (a) shows the energy by position inside the sample, while the emitted CL intensity was plotted against the penetration depth in the sample in Fig. 5(b). The red dashed line indicates the 8nm layer depth in both figures. The characteristic pear-shaped interaction volume is well observed in Fig. 5 (a). This figure illustrates the respective contribution of the substrate and of the layer to the resulting CL spectrum. Indeed, integrating over the areas in Fig. 5 (b), a 5% of the total CL signal is coming from the first 8 nm depth. Assuming a deposition of 8 nm thick $2x10^{17}$ cm^{-3} boron doped diamond, the hypothetical resulting CL spectrum should correspond to that of a $10^{16}cm^{-3}$ doping level (i.e. 20 time less, a 5%) recorded on a thick (>250 nm) diamond layer. This is clearly not the case as the experimentally obtained spectrum corresponds to a $3x10^{15}cm^{-3}$ boron doping level. Thus, using a e-beam accelerating voltage of 5 kV, CL is sufficiently sensitive to detect an 8 nm-thick $2x10^{17}$ cm^{-3} doped layer if it were present. Taking this into account and considering that the doping level deduced from the CL spectrum of region E corresponds to that of the residual boron doping of the reactor, we can stand that, in the present case, not any boron-doped layer was deposited on the {100}-oriented surface. In the same way, doping values obtained for position F were likely underestimated because of the doped layer was probably thinner than 200 nm and of the spectral

contribution from the intrinsic layer placed below.

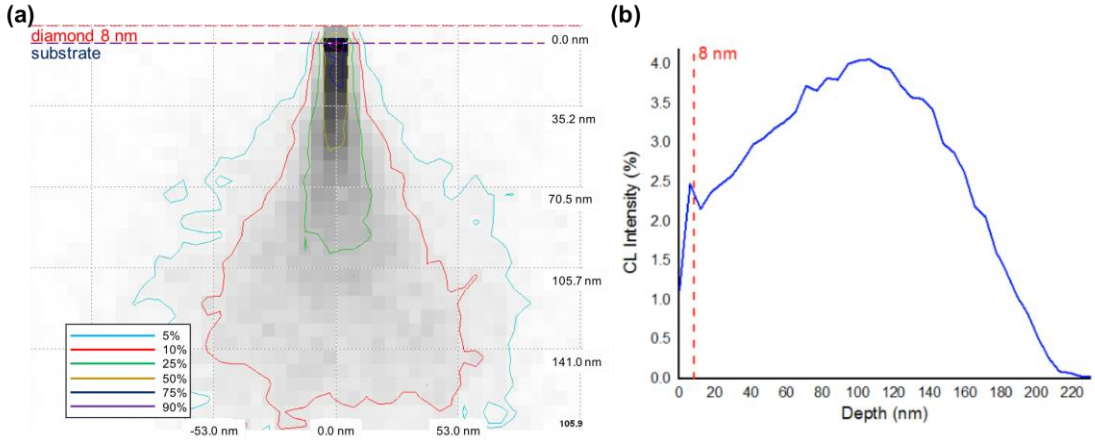

Figure 5. (a) Monte Carlo simulation of the energy by position in a 5 keV accelerating voltage beam impinging a bi-layered diamond sample. **(b)** CL intensity per depth of the same simulation.

This work demonstrates that selective doping is possible over patterned substrate along specific orientations using growth conditions maximizing the dependence of the growth rate on the growth orientation. A longer growth would eventually result in planarized 100-oriented layers with buried 3D locally doped regions. Subsequent etching processes that can be undertaken in the same CVD reactor using an O_2 plasma would provide access to these regions while maintaining the planar surface. Therefore, this result paves the way for power electronic device designs where photolithography steps should be avoided.

ACKNOWLEDGEMENTS

This work has been co-financed by the 2014-2020 ERDF Operational Programme and by the Department of Economy, Knowledge, Business and University of the Regional Government of Andalusia. Project reference: FEDER-UCA18-107851. Authors also want to thank the Ministerio de Economia y Competitividad (MINECO) of the Spanish Government for funding under Grant No. TEC2017-86347-C2-1-R and NºESP2017-91820-EXP.

DATA AVAILABLITY

The data that support the findings of this study are available from the corresponding author upon reasonable

request.

REFERENCES

1. N. Donato, N. Rouger, J. Pernot, G. Longobardi, F. Udrea, J. Phys. D: Appl. Phys, 53, 9, 093001 (2019)
2. A. Aleksov, M. Kubovic, N. Kaeb, U. Spitzberg, A. Bergmaier, G. Dollinger, Th. Bauer, M. Schreck, B. Stritzker, E. Kohn, Diam. Relat. Mater., 12, 391-398 (2003).
3. A. Tallaire, O. Brinza, V. Mille, L. William, and J. Achard, Adv. Mater., 1604823 (2017)
4. H. Umezawa, M. Nagase, Y. Kato, andS. Shikata, Diam. Relat. Mater., 24, 201 (2012)
5. Y. Hoshino, H. Kato, T. Makino, M. Ogura, T. Iwasaki, M. Hatano, and S. Yamasaki, Phys. Status Solidi A, 209 (9), 1761 (2012)
6. K. Sato, T. Iwasaki, Y. Hoshino, H. Kato, T. Makino, M. Ogura, S. Yamasaki, S. Nakamura, J. Ichikawa, A. Sawabe, and M. Hatano, Jap. J. Appl. Phys., 53, 05FP01 (2014).
7. G. Biasol, A. Gustafsson, K. Leifer, and E. Kapon, Phys. Rev. B, 65, 205306 (2002)
8. H. Kato, T. Makino, M. Ogura, D. Takeuchi, and S. Yamasaki, Diam. Relat. Mater., 19. 27 (2012)
9. Y. Ando, T. Kamano, K. Suzuki, and A. Sawabe, Jap. J. Appl. Phys., 51, 090101 (2012)
10. D. Takeuchi, T. Makino, H. Kato, M. Ogura, N. Tokuda, T. Matsumoto, D. Kuwabara, H. Okushi, and S. Yamasaki, Physica status Solidi A, 211, 2251 (2014)
11. F. Lloret, A. Fiori, D. Araujo, D. Eon, M.P. Villar, and E. Bustarret, Appl. Phys. Lett. 108, 181901 (2016).
12. F. Lloret, D. Araujo, D. Eon, and E. Bustarret, Cryst. Growth Des., *Crystal Growth & Design 18*, 12, 7628-7632 (2018).
13. A. Boussadi, A. Tallaire, M. Kasu, J. Barjon, J. Achard, Diam. Relat. Mater., 83, 162 (2018)
14. F. Lloret, M. Gutierrez, D. Araujo, D. Eon, and E. Bustarret, Phys. Status Solidi A, 214, 1700242 (2017)
15. C. Baron, M. Wade, A. Deneuville, F. Jomard, J. Chevallier, Diam. Relat. Mater., 15, 597 (2006)
16. S. Ghodbane, F. Omnès, C. Agnès, Diam. Relat. Mater., 19, 273 (2010)
17. A. Deneuville, C. Baron, S, Ghodbane, C. Agnès, Diam. Relat. Mater., 16, 915 (2007).

18. C. Baron, M. Wade, A. Deneuville, E. Bustarret, T. Kocinievski, J. Chevalier, C. Uzan-Saguy, R. Kalish, J. Butler, Diam. Relat. Mater., 14, 350 (2005).
19. J. Barjon, Phys. Status Solidi A, 214, 1700402 (2017).
20. F. Lloret, D. Araujo, D. Eon, M.P. Villar, J.M. Gonzalez-Leal, E. Bustarret, Phys. Stat. Solidi A, 213, 10, 2570 (2016).
21. F. Omnès, P. Muret, P.-N. Volpe, M. Wade, J. Pernot, F. Jomard, Diam. Relat. Mater., 20, 912 (2011)
22. Y. Zou and K. Larsson, J. Phy. Chem. C, 120, 10658 (2016)

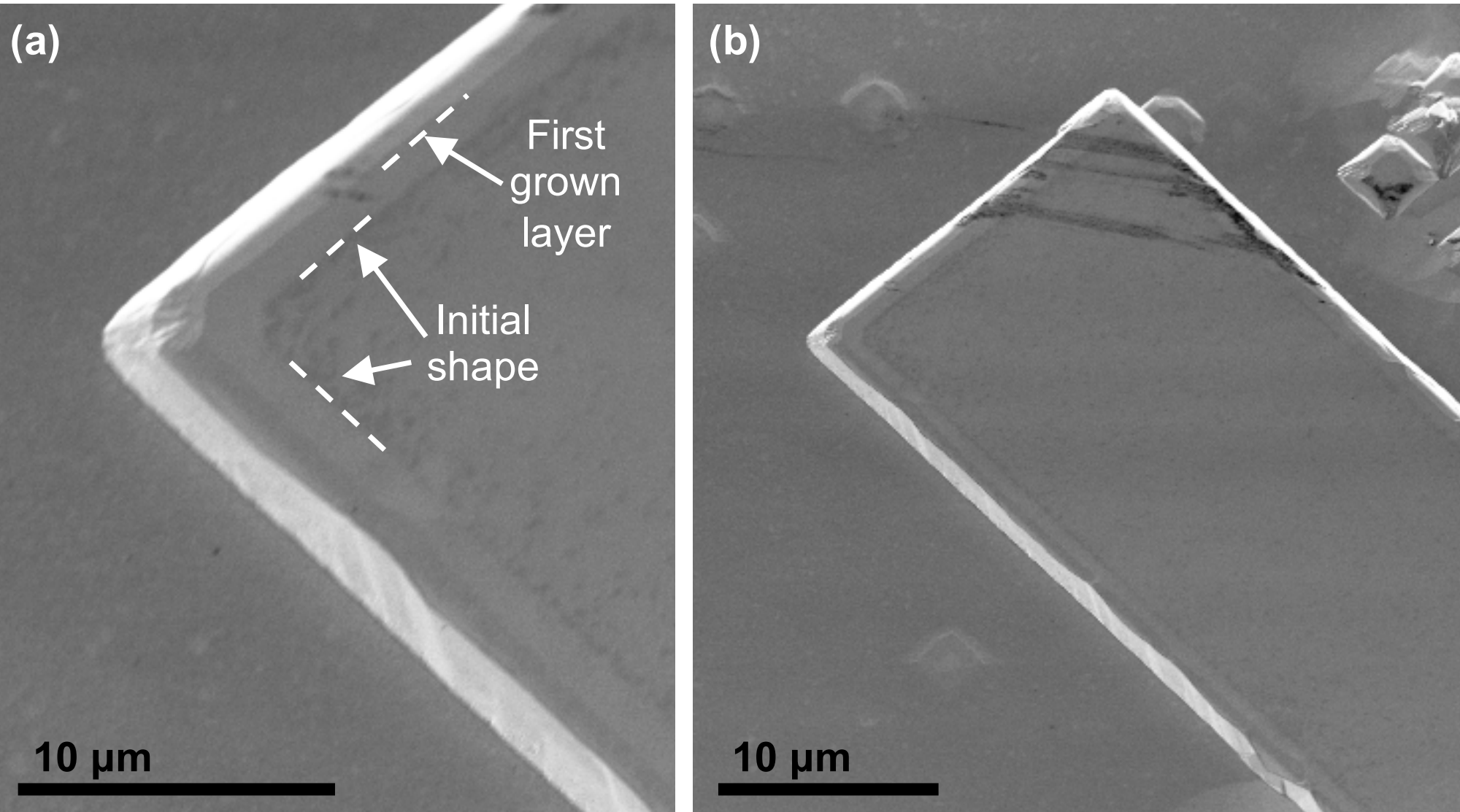
(a)
First grown layer
Initial shape
10 µm
(b)
10 µm

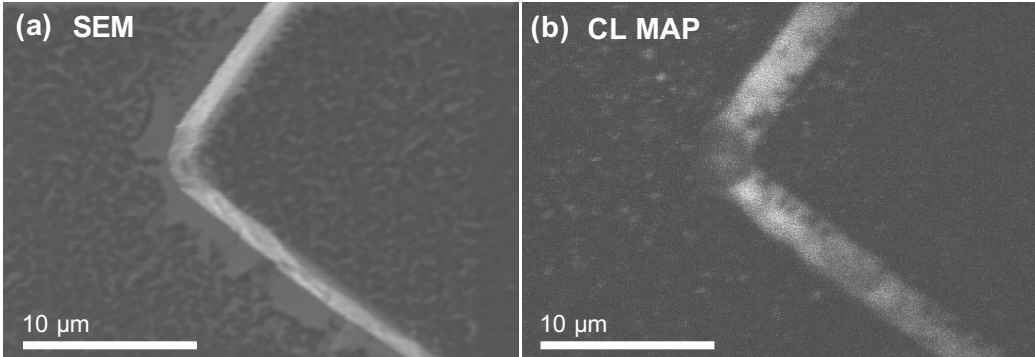
(a) SEM
10 μm
(b) CL MAP
10 μm

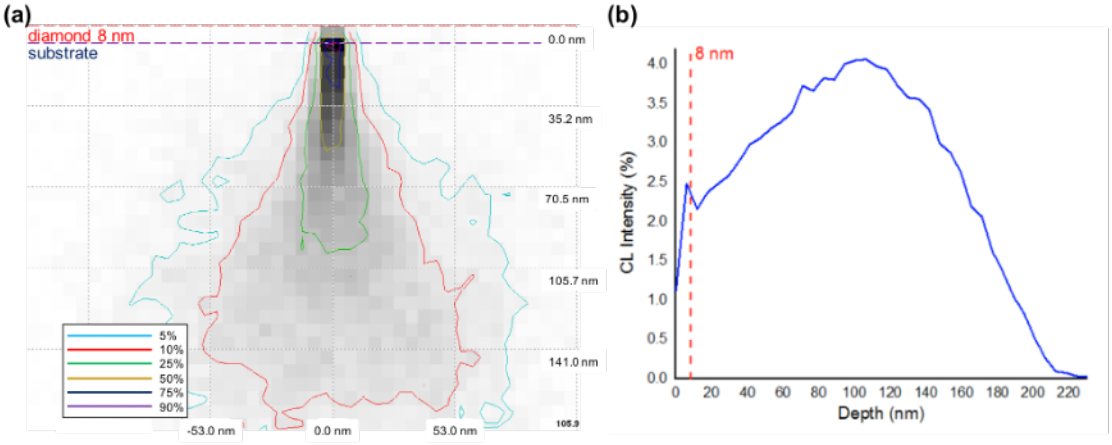
(a)
diamond 8 nm
substrate
0.0 nm
35.2 nm
70.5 nm
105.7 nm
141.0 nm
5%
10%
25%
50%
75%
90%
-53.0 nm
0.0 nm
53.0 nm
(b)
8 nm
CL Intensity (%)
Depth (nm)

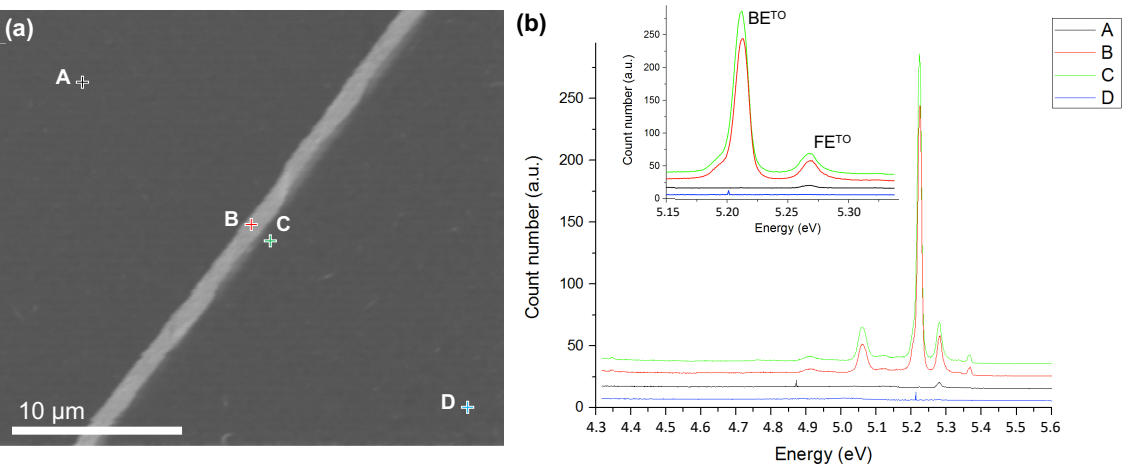
(a)
A
B
C
D
10 µm
(b)
BE^TO
FE^TO
A
B
C
D
Count number (a.u.)
Energy (eV)
0
50
100
150
200
250
4.3
4.4
4.5
4.6
4.7
4.8
4.9
5.0
5.1
5.2
5.3
5.4
5.5
5.6
5.15
5.20
5.25
5.30

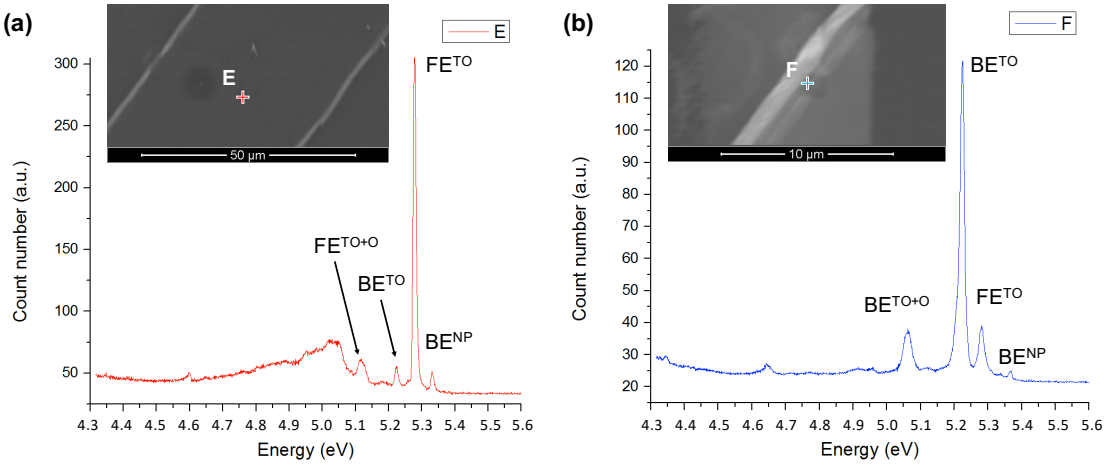
(a)
E
E
50 µm
FE^TO
FE^TO+O
BE^TO
BE^NP
Count number (a.u.)
Energy (eV)
(b)
F
F
10 µm
BE^TO
BE^TO+O
FE^TO
BE^NP
Count number (a.u.)
Energy (eV)